Eur. J. Mineral.
2001, **13**, 621-634

Carbonate and silicate phase reactions during ceramic firing

GIUSEPPE CULTRONE(1), CARLOS RODRIGUEZ-NAVARRO(1)*, EDUARDO SEBASTIAN(1),
OLGA CAZALLA(1) AND MARIA JOSE DE LA TORRE(2)

(1) Departamento de Mineralogía y Petrología - Universidad de Granada
Fuente Nueva s/n - 18002 Granada, Spain
(2) Departamento de Geología Universidad de Jaén, Spain

Abstract: Mineralogical, textural and chemical analyses of clay-rich materials following firing, evidence that initial mineralogical differences between two raw materials (one with carbonates and the other without) influence the textural and mineralogical evolution of the ceramics as *T* increases from 700 to 1100°C. Mineralogical and textural changes are interpreted considering local marked disequilibria in a system that resembles a small-scale high-*T* metamorphic process (*e.g.*, contact aureoles in pyrometamorphism). In such conditions, rapid heating induces significant overstepping in mineral reaction, preventing stable phase formation and favoring metastable ones. High-*T* transformations in non-carbonate materials include microcline structure collapse and/or partial transformation into sanidine; and mullite plus sanidine formation at the expenses of muscovite and/or illite at $T \geq 800°C$. Mullite forms by muscovite-out topotactic replacement, following the orientation of mica crystals: *i.e.*, former $(001)_{muscovite}$ are $\perp$ to $(001)_{mullite}$. This reaction is favored by minimization of free energy during phase transition. Partial melting followed by fingered structure development at the carbonate-silicate reaction interface enhanced high-*T* Ca (and Mg) silicates formation in carbonate-rich materials. Gehlenite, wollastonite, diopside, and anorthite form at carbonate-silicate interfaces by combined mass transport (viscous flow) and reaction-diffusion processes. These results may add to a better understanding of the complex high-*T* transformations of silicate phases in both natural (*e.g.*, pyrometamorphism) and artificial (*e.g.*, ceramic processing) systems. This information is important to elucidate technological achievements and raw material sources of ancient civilizations and, it can also be used to select appropriate clay composition and firing temperatures for new bricks used in cultural heritage conservation interventions.

Key-words: Ceramics, carbonates, clay, high-*T* reactions, gehlenite, mullite, wollastonite, reaction-diffusion fingers, muscovite-out reaction, architectural conservation.

1. Introduction

The hardening reaction taking place when a clay-rich sediment is fired is a fundamental characteristic of ceramic technology since the prehistory. This process occurs by high-*T,* low-*P* mineral transformations that are mainly influenced by the mineralogical composition of the raw clay-rich material, its granulometry, the firing temperature, as well as the kiln (oven) atmosphere conditions (Maggetti, 1982).

Previous works have studied the mineralogical and textural changes taking place following firing of raw clay (Tite & Maniatis, 1975; Freestone & Middleton, 1987; Veniale, 1990; Duminuco *et al.*, 1996; Riccardi *et al.*, 1999), as well as the mineralogical and structural modifications induced by the presence of carbonates in the paste (Rye, 1976; Peters & Iberg, 1978; Maggetti, 1982). Even though, some reactions taking place when single phases form at high temperature (T > 750°C) are well-established (Peters & Iberg, 1978), the influ-

---

*E-mail: carlosrn@goliat.ugr.es

DOI: 10.1127/0935-1221/2001/0013-0621 0935-1221/01/0013-0621 $ 3.50

ence of and the interactions between various phases that coexist, disappear, or form, are not well established. Little is known on the transformations undergone by silicate and carbonate phases at the reaction interfaces, or the phyllosilicate-out reaction. In particular, there is no clear understanding of the transport mechanisms of reactants (*i.e.*, diffusion *vs.* mass transport/viscous flow) and the processes involved in mineral transformation at high-*T* (*i.e.*, solid-state reactions *vs.* crystallization from a melt). These issues are not solely relevant for understanding ceramics, as there is a close similarity between ceramic formation and the development of reaction textures resulting from marked disequilibrium during pyrometamorphism (*i.e.*, in contact aureoles or in xenoliths where heating rates were very rapid; Brearley, 1986, Brearley & Rubie, 1990; Preston *et al.*, 1999). They also may have important implications in understanding ancient ceramic technologies, or elucidating raw material sources, as well as in the designing of new ceramic materials in general, or appropriate (*i.e.*, compatible) conservation materials (*i.e.*, bricks) for architectural heritage conservation interventions.

It is the aim of this work to study the mineralogical, chemical and textural changes of both residual minerals and newly formed phases taking place upon firing, and, in particular, the mechanisms of mineral transformation of raw clay-rich materials with and without carbonates.

2. Materials and methods

Two Pliocene clay-rich materials were selected, one from Guadix (G) and the other form Viznar (V), two villages located in the vicinity of Granada, Spain. Raw material was collected, milled and sieved, discarding the fraction with grain size > 1.5 mm. Bricks paste was prepared adding 400 cc of water to 1000 g of raw material. G and V bricks were fashioned using a wooden mould 24.5 × 11.5 × 4 cm in size, and fired in an air-ventilated electric oven (Hoerotec, CR-35) at the following temperatures: 700, 800, 900, 1000, and 1100°C. *T* was raised at a heating rate of 3°C per minute, first up to 100°C with one hour soaking time, and later up to the peak *T* with a soaking time of three hours. Fired brick samples were stored at constant *T* and relative humidity (RH) conditions of 21°C and 55 %, respectively.

Separation of the fractions < 2 µm, 2 to 20, and > 20 µm was performed using a KUBOTA 2000 centrifuge. Grain size distribution in the < 20 µm fraction was determined using a laser-beam particle size analyzer (GALAI^h CIS-1). Grain size distribution of > 20 µm fraction was determined using standard ASTM sieves (50 µm up to 1 mm mesh ϕ).

The mineralogy of the raw material as well as the mineralogical changes taking place upon firing were studied by powder X-ray diffraction (XRD) using a Philips PW-1710 diffractometer with automatic slit, Cu$K\alpha$ radiation ($\lambda = 1.5405$), 3 to 60°2θ explored area, and 0.01°2θ s^{-1} goniometer speed. At least three samples (~ 1 g each) of each brick type/firing *T* were analyzed. They were milled in agate mortar to < 40 µm particle size. XRD analysis of the clay fraction (*i.e.*, fraction with grain size < 2 µm) was performed using oriented aggregates (air-dried, ethylene-glycol and dimethyl sulfoxide solvated, and 1 h heated at 550°C).

The bricks texture and microstructure, as well as the progress of mineral transformation and reactions upon firing, were studied by means of optical microscopy (OM) and scanning electron microscopy (SEM; Zeiss DMS 950) coupled with EDX microanalysis. Two thin sections per sample type and firing *T* were prepared. A polished thin section was prepared using one of them. Both, SEM secondary electron (SE) and back-scattered electron (BSE) images were acquired using either small brick pieces (5 × 5 × 10 mm in size; gold coated), or polished thin sections (carbon coated). The same thin sections were used to analyze small-scale compositional changes of selected minerals following firing by means of an electron microprobe (EMPA; Cameca SX 50). The EMPA working conditions were 20 keV beam energy, 0.7 mA filament current, and 2 µm spot-size diameter. 14 analyses of muscovite crystals (4/700°C; 6/800°C, and 4/1100°C) and 25 of carbonates (6/700°C; 9/800°C, and 10/1100°C) were performed. Albite, orthoclase, periclase, wollastonite and oxides (Al_2O_3, Fe_2O_3, and $MnTiO_2$) were used as standards (Govindaraju, 1989). Detection limit for major elements after ZAF correction (Scott & Love, 1983) was 0.01 wt %.

Bulk chemical analyses of ceramic materials before and after firing at each target *T* were performed by means of X-ray fluorescence (XRF; Philips PW-1480). 1 g per raw material or fired brick sample was finely ground and well mixed in agate mortar before being pressed into Al holder for disk preparation. ZAF correction was performed systematically (Scott & Love, 1983). International standards (Govindaraju, 1989) were used thoroughly. The estimated detection limit for major elements was 0.01 wt %.

3. Results

3.1. Granulometry

V samples show a higher concentration of particles < 2 µm when compared with G samples (Fig. 1). However, the differences are not significant. Both samples show a maximum in particle size around 100 µm. Carbonates are the most abundant phase in the larger size fraction in V samples, while schist pieces (with Ms plus Qtz and Fs; mineral symbols after Kretz (1983)) made up the larger size fraction of G samples.

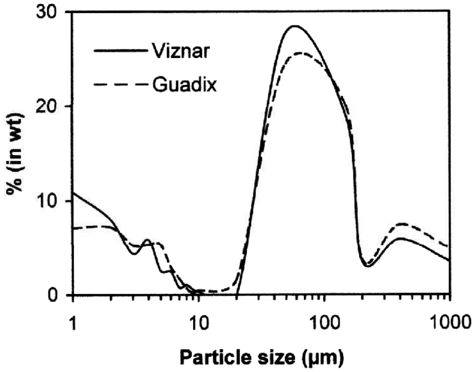

Fig. 1. Grain-size distribution curves for Guadix and Viznar raw material.

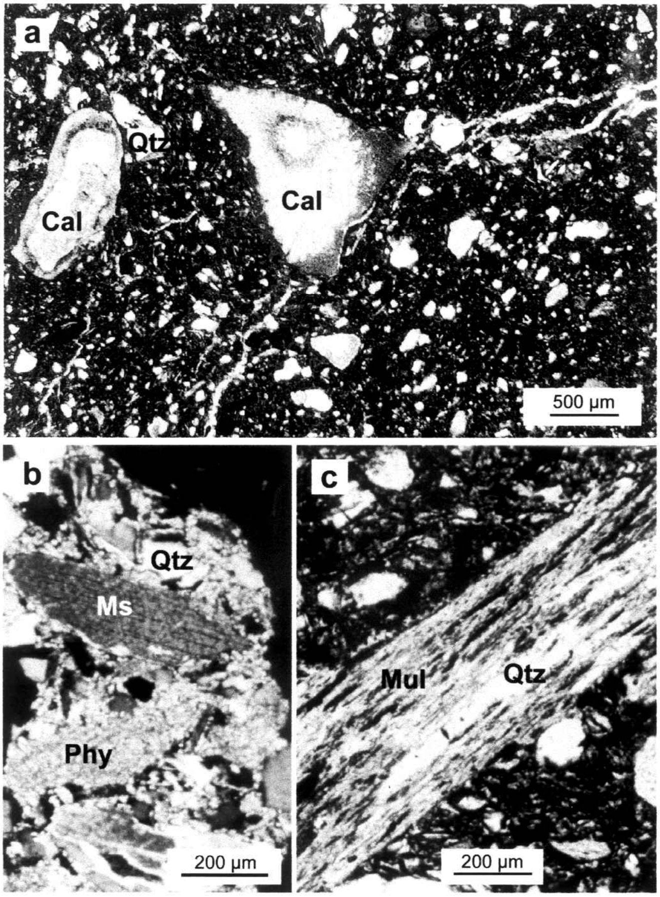

Fig. 2. Optical microscopy micrographs of: a) calcite (Cal) grain fired at 800°C showing cracks which penetrates the brick matrix (plane light). Reaction rims are observed at the carbonate-phyllosilicate (matrix) and carbonate-quartz (Qtz) interfaces; and b) muscovite (Ms) crystal before (cross polars) and c) after heating up to 800°C (plane light). Mullite (Mul) observed in the latter.

3.2. Optical microscopy analysis

G and V samples fired at 700°C do not show significant mineralogical transformations. The temper grain-size (*i.e.*, phenocrysts) reaches up to 1.5 mm. No major textural changes are visible in the carbonates at 700°C. Phyllosilicates in the paste are oriented due to compression during molding. At 800°C carbonate decomposition in V samples is almost complete and some cracks appear surrounding the former carbonate grains (Fig. 2a). The matrix in both G and V samples turns dark with low birefringence as T increases. Muscovite crystals in both G and V samples start to transform into mullite at 800°C, and some bubbles develop within these crystals at higher T (Fig. 2b and 2c). Muscovite replacement by mullite is completed at 1000°C. Mullite preserves the morphology of replaced muscovite. In fact, mullite (001) planes are ⊥ to (001) planes of former muscovite grains, as deduced by the optical axes orientation study. At 1000-1100°C the matrix is fully vitrified and brown colored (in both G and V samples). Phyllosilicates in the matrix do not exist at these T, only some pseudomorphs after former crystals can be observed. An empty space with scattered grayish fragments at the pore edges can be found where calcite was originally present. Cracks observed in V samples at $T < 900$°C disappear at 1100°C due to extended vitrification. Pores become more abundant, and they are no longer ellipsoidal but spherical. However, an orientation of the remaining temper grains in planes parallel to the brick largest faces (*i.e.*, where compression was applied during molding) remains.

3.3. XRD analysis

Raw G samples show significant amounts of quartz and phyllosilicates with little feldspar. The < 2 µm fraction includes illite and smectite with small amounts of kaolinite and paragonite (Table 1). There is no chlorite, which could have been masked by the $d_{(001)}$ peaks of smectite (~ 14 Å) and kaolinite (7.1 Å), as evidenced by these peaks disappearing after 90´ heating at 550°C. Raw V samples have significant amounts of calcite and dolomite. The clay fraction includes illite and smectite with trace amounts of paragonite and kaolinite (Table 1). Therefore, the main difference among the two raw materials lays in the mineralogical composition of the > 2 µm fraction.

Regarding the phyllosilicates evolution upon firing, only the diffraction peak at 10 Å, corresponding to a dehydroxylated illite-like phase, remains at 700°C. This peak intensity is reduced upon firing at higher T, till it disappears at ~ 900°C (Fig. 3a and 3b). Microcline main diffraction peak reduces its intensity in G samples. This mineral disappears at $T > 1000$°C when trace amounts of sanidine are formed. Mullite is detected in both G and V samples at $T \sim 900$°C, increasing its main diffraction peak ($d_{(210)} = 3.39$ Å) intensity at higher T. Mullite diffraction peaks are more intense in phyllosilicate-rich G samples than in carbonate-rich V samples. Other phases undergo a significant increase in their diffraction peaks intensities: this is the case of hematites in G samples fired at $T > 1000$°C. New phases appear in V samples upon firing: a) gehlenite (a melilite-group phase) appears at 800°C, increasing its main Bragg peak intensity at 900°C and reducing it at higher T; b) wollastonite and diopside appear at 1000°C and they show a significant increase in their main diffraction peak at higher T. Decomposition of calcite and dolomite begins at $T > 700$°C and both phases disappear at $T > 800$°C. Quartz remains as the most abundant phase at any T in both V and G samples. In V samples the plagioclase increases its Ca content (*i.e.*, a more An-rich phase), as well as its main Bragg peak intensity as T increases. This increase is more significant at $T > 1000$°C. The existence of an amorphous phase (*i.e.*, vitreous phase) is evidenced by

Table 1. Results of XRD analysis of the raw materials and the fraction with < 2 µm grain size. Mineral symbols after Kretz (1983), (in Table 3).

Whole sample	Qtz	Phy	Fs	Cal	Dol
GUADIX	****	***	*	-	-
VIZNAR	***	***	*	**	**

< 2 µm	Sm	Ill	Kln	Pg
GUADIX	***	***	**	*
VIZNAR	***	***	**	**

****= very abundant; ***=abundant; **=scarce; *=trace; - = not detected.

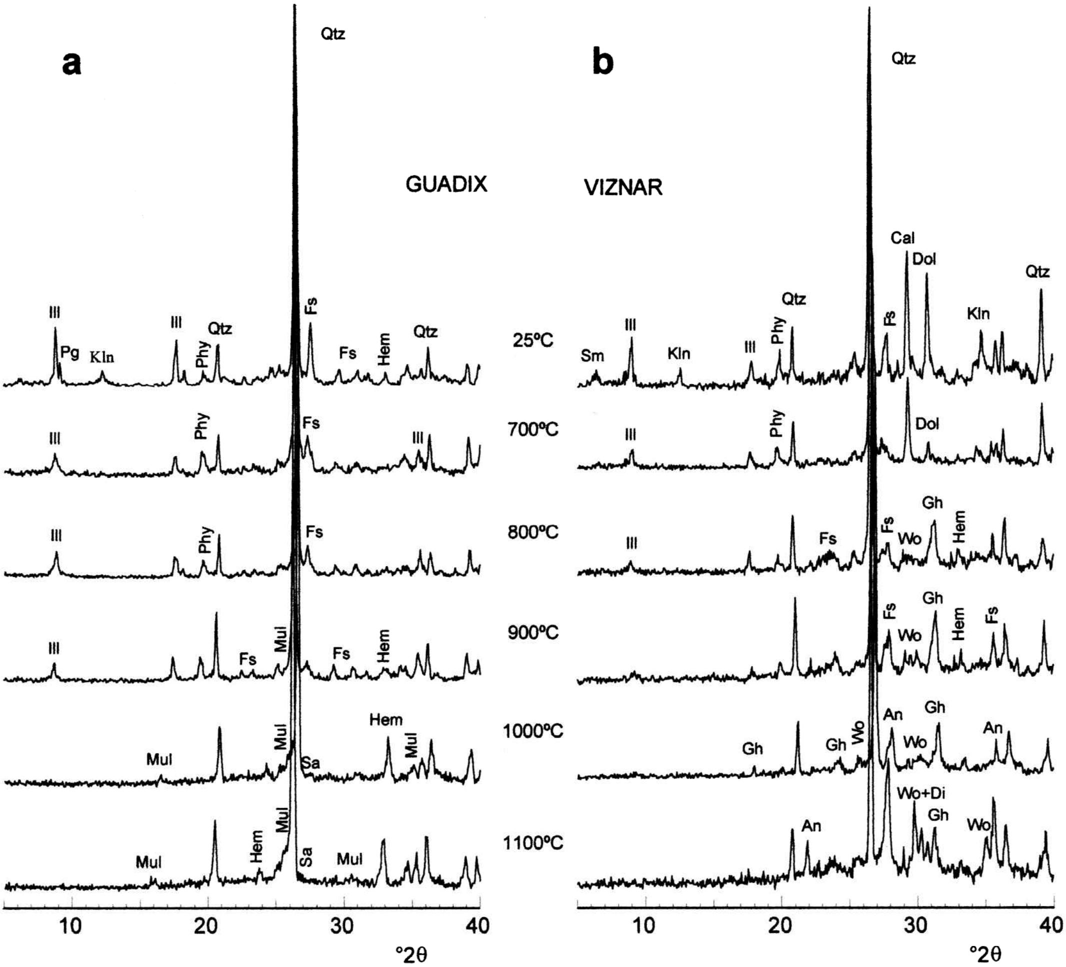

Fig. 3. Guadix (a) and Viznar (b) samples powder X-ray difraction patterns. Legend (mineral symbols after Kretz, 1983): Sm = smectite; Ill = illite; Pg = paragonite; Qtz = quartz; Cal = calcite; Kln = kaolinite; Phy = phyllosilicates; Fs = feldspar; Dol = dolomite; Gh = gehlenite; Hem = hematite; Wo = wollastonite; Di = diopside; An = anorthite; Mul = mullite; Sa = sanidine. Cu*K*α X-ray radiation, λ = 1.5064 Å.

a rise of the background noise in the XRD pattern at $T > 900$°C in the G samples, and at $T > 800$°C in the V samples.

3.4. SEM-EDX analysis

Significant textural changes, most evident with respect to pore morphology and volume, were detected upon firing. An overall porosity reduction is observed at $T > 1000$°C when the vitreous phase fills the pores.

Samples fired at 700 and 800°C still preserve the laminar habit of phyllosilicates, although muscovite crystals clearly exfoliate along basal planes, most probably due to dehydroxylation (Fig. 4a). The interlocking among particles is limited (Fig. 4d). V samples show some cracks. At these T no clear evidence of sintering or partial melting is detected. However, there is indirect evidence (*i.e.*, increase in background noise of XRD patterns) that some vitrification is reached at $T < 900$°C in carbonate-rich V samples. Vitrification is clearly observed in all samples at $T > 900$°C: *i.e.*, phyllosilicates appear deformed (their edges turn smooth) and/or aggregated (Fig. 4b and 4e), and the pores turn ellipsoidal with smooth surfaces. At $T > 1000$°C these effects are less extended in the carbonate-rich V samples (Fig. 4c) than in the sil-

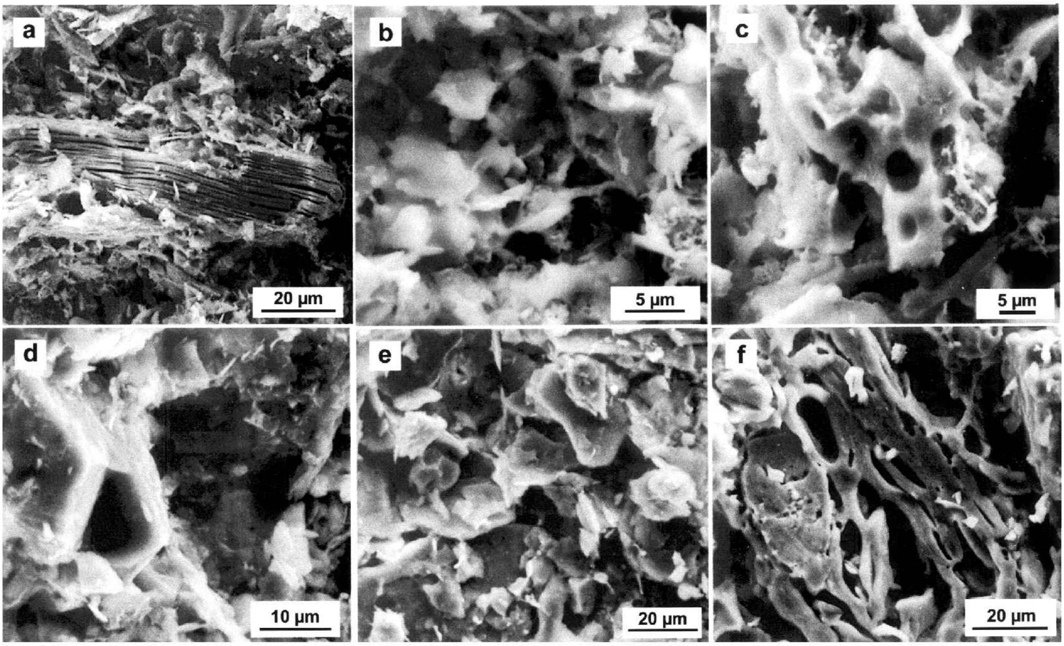

Fig. 4. SEM secondary electron photomicrographs of Viznar samples fired at 800°C (a), 1000°C (b), and 1100°C (c); and Guadix samples fired at 700°C (d), 900°C (e) and 1000°C (f).

icate-rich G samples (Fig. 4f). A higher degree of particle interlocking results in a porosity reduction. At 1100°C vitrification is significant in all samples regardless of initial compositional differences. Pores coalesce as spherical cells due to partial or extended melting of clay particles in the matrix.

BSE images of mineral and textural evolution of samples with high carbonate content (*i.e.*, V samples, which undergo the most significant mineralogical changes) give an interesting picture of local phase transformations taking place at grain boundaries. No textural or mineralogical changes can be detected in brick fired at 700°C (Fig. 5a). Carbonates comprise the larger-size fraction in these samples, which allows easy detection of high-*T* reaction rims. In fact, at 800°C, 2-5 µm thick reaction rims are observed developing at the calcite-quartz/phyllosilicate interface (Fig. 5b). Rims composition corresponds to a calcium silicate phase, presumably wollastonite (EDX results). A dark rim surrounded by a light outer shell is observed where dolomite was originally present (Fig. 5c). However, no compositional variation among internal (greyish) and external (white) rims is detected. We were not able to unambiguously detect the presence of gehlenite within these reaction rims (*i.e.*, some EDX analyses of 2-5 µm thick rims at the carbonate-silicate interface showed Al together with Ca and Si, but possible contamination from underlying phyllosilicates was not discarded). However, the presence of gehlenite was detected by XRD at this *T* (800°C). Muscovite phenocrysts (Fig. 5d) show a morphology and composition typical for unaltered white mica. At 1100°C muscovite crystals show secondary bubbles development between layers (Fig. 5e). The mica composition is homogeneous (no BSE image gray-level differences along the crystals) and it is similar to that of an unchanged muscovite, but with slightly lower K concentration. At 1100°C, carbonates (*i.e*., dolomite in Fig. 5f) shows an outer thick white Ca- and Si-rich rim (*i.e.*, wollastonite) which includes small (micron sized) bright-white Ca-, Si- and Al-rich particles (*i.e.*, gehlenite or plagioclase). There is a striking feature of this reaction rim: it shows a fingered geometry at the outer edge. The darker dolomite core shows a significant Mg enrichment.

3.5. EMPA analysis

Due to the fact that only silicate phases in samples with carbonates undergo mayor composition-

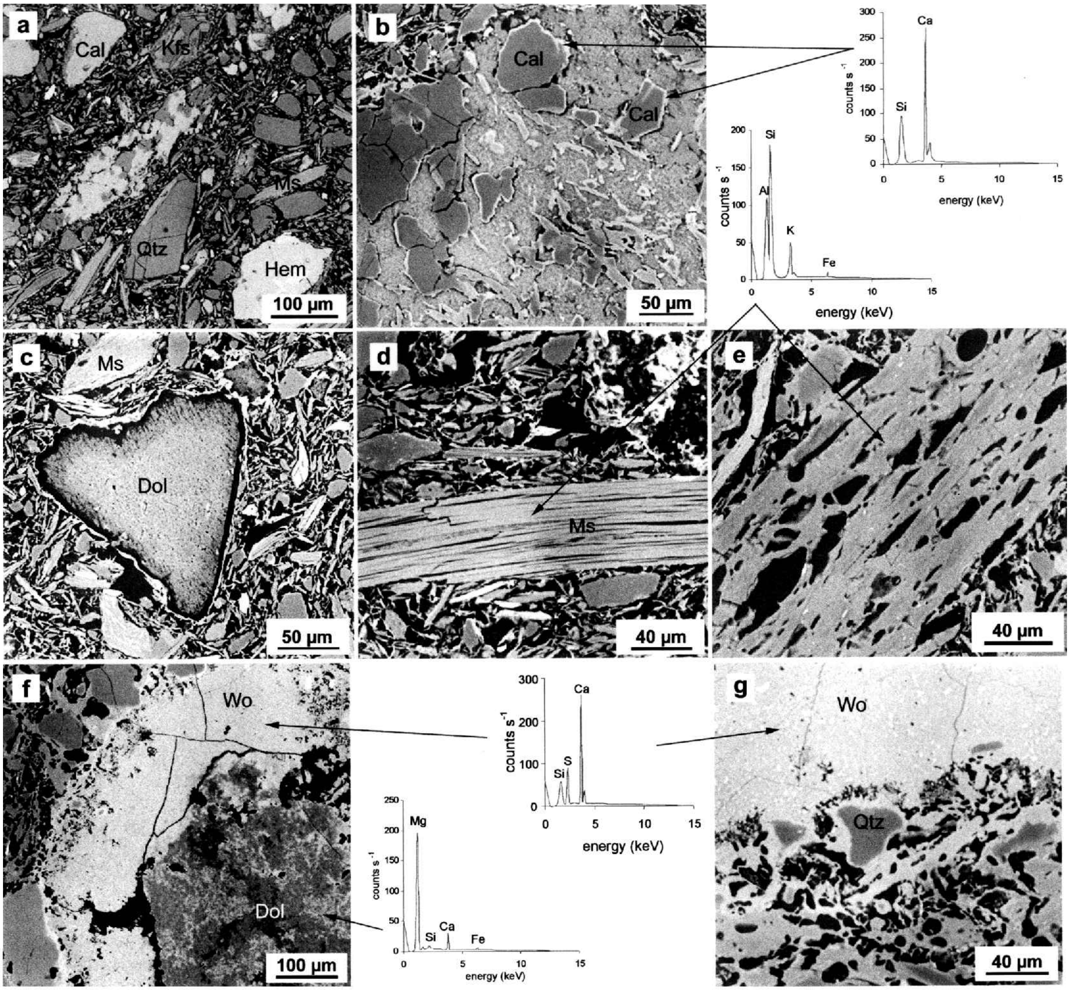

Fig. 5. BSE images and EDX analyses of carbonate-rich Viznar samples: a) fired at 700°C; b) fired at 800°C, when Wo (EDX analysis) formed at the Cal- silicates interface; c) detail of former carbonate grain showing a white outer reaction rim (Wo or Gh?), a crack, and an inner core with an outer darker shell (see text for details); d) Ms (see EDX analysis) at 700°C; e) former Ms after transformation into a Fs? + Mul + melt mixture (see EDX analysis); f) Dol/Phy (+ Qtz) interface showing a reaction rim with fingered geometry formed at 1100°C; g) detail of the outer reaction rim in previous figure; EDX analysis shows the rim composition (*i.e.*, Wo).

al changes upon firing, only V samples were analyzed using this technique. In particular, compositional changes of phyllosilicates and carbonates were studied using polished thin sections of fired V bricks (one section per selected target *T*: *i.e.*, 700, 800, 1100°C).

Phyllosilicates (Table 2) show a muscovitic composition at 700°C, where some K is replaced by Na, even though, the overall composition does not seem to correspond to paragonite. Nevertheless, paragonite was detected in the raw clay (Fig. 3b). Fe, Mg and Ti replace some Al in the octahedral sheets. Replacement of OH^- by F^- is almost absent. At 800°C a slight increase in Fe content is detected. Only analyses M9 and M10 show higher concentrations of Na and Al. At 1100°C the amount of K is reduced, while Ca and Si content is increased. The total oxide content is close to 100 %, a value consistent with complete dehydroxylation of the phyllosilicates. Analyses M11-M14 in Table 2 are in agreement with high-*T* phengite compositional data from Worden *et al.* (1987).

Table 2. EMPA analysis results of phyllosilicates composition (in wt %).

T	700 °C				800 °C						1100 °C			
Analysis	M1	M2	M3	M4	M5	M6	M7	M8	M9	M10	M11	M12	M13	M14
SiO_2	47.18	47.59	50.99	49.46	48.39	48.31	49.76	46.55	49.55	48.03	56.56	57.11	51.03	50.49
TiO_2	0.33	0.37	0.25	0.33	0.39	0.36	0.24	0.43	0.39	0.24	1.77	0.55	0.36	0.34
Al_2O_3	34.78	34.46	28.38	31.82	28.01	28.44	28.38	28.67	33.68	37.23	31.25	32.46	33.71	32.85
Cr_2O_3	0.00	0.01	0.00	0.04	0.00	0.00	0.02	0.06	0.02	0.03	0.03	0.01	0.00	0.00
FeO	1.55	1.64	2.18	1.56	3.99	4.14	3.74	3.43	2.17	1.52	1.14	1.21	3.10	2.96
MnO	0.01	0.00	0.00	0.02	0.01	0.01	0.02	0.00	0.00	0.18	0.02	0.00	0.05	0.03
MgO	1.01	1.21	3.02	2.30	2.55	2.59	3.02	1.89	1.69	0.69	0.79	0.68	2.12	2.08
CaO	0.03	0.02	0.00	0.00	0.03	0.11	0.03	0.05	0.02	0.16	0.31	0.29	1.69	1.56
Na_2O	1.04	1.20	0.41	0.86	1.13	0.81	0.80	0.61	1.25	2.74	0.97	1.01	1.29	1.35
K_2O	9.29	8.97	9.23	8.77	9.67	9.84	10.36	9.90	9.40	7.78	6.54	6.71	7.54	8.43
NiO	0.00	0.00	0.02	0.00	0.04	0.02	0.01	0.01	0.01	0.01	0.01	0.01	0.00	0.03
F	0.05	0.13	0.19	0.14	0.07	0.10	0.05	0.21	0.03	0.00	0.08	0.09	0.04	0.04
Cl	0.00	0.01	0.00	0.00	0.01	0.01	0.02	0.04	0.01	0.02	0.00	0.00	0.00	0.01
Total	95.26	95.60	94.67	95.29	94.29	94.74	96.44	91.85	98.20	98.63	99.48	100.10	100.90	100.10

Table 3. Composition of selected carbonate grains (EMPA results in wt %).

T	700 °C			800 °C				1100°C					
Analysis	C3	C4	C6	C8	C10	C12	C14	C16	C17	C18	C20	C22	C25
SiO_2	0.00	0.00	0.01	6.42	18.97	0.04	0.07	8.86	19.24	32.84	24.89	0.36	0.03
TiO_2	0.00	0.02	0.00	0.06	0.25	0.00	0.00	0.03	0.22	0.21	0.08	0.04	0.00
Al_2O_3	0.00	0.00	0.00	3.38	7.28	0.01	0.05	0.19	4.02	18.99	12.92	0.34	0.11
Cr_2O_3	0.00	0.00	0.00	0.01	0.01	0.00	0.00	0.03	0.05	0.02	0.00	0.02	0.00
FeO	0.00	0.01	0.03	0.76	3.59	0.01	0.00	0.49	2.39	4.73	1.64	0.85	0.15
MnO	0.00	0.02	0.00	0.34	0.31	0.00	0.00	0.01	0.03	0.04	0.05	0.05	0.00
MgO	0.38	1.04	0.00	0.81	2.29	0.00	30.28	52.48	5.30	1.77	0.07	78.96	68.97
CaO	54.12	53.23	36.37	52.04	44.12	35.95	39.02	26.85	38.76	18.75	56.99	4.25	22.58
Na_2O	0.00	0.00	0.02	0.06	0.16	0.02	0.01	0.02	0.01	0.41	0.02	0.00	0.01
K_2O	0.01	0.00	0.00	0.04	0.11	0.01	0.00	0.01	0.02	0.30	0.00	0.00	0.00
NiO	0.02	0.01	0.00	0.02	0.00	0.00	0.01	0.00	0.00	0.03	0.04	0.01	0.00
F	0.00	0.00	0.00	0.27	0.09	0.00	0.55	1.04	1.39	0.03	0.37	0.00	9.57
Cl	0.01	0.01	0.04	0.04	0.08	0.03	0.04	0.07	0.08	0.04	0.83	0.04	0.04
Total	54.54	54.34	36.47	64.25	77.26	36.07	70.03	90.08	71.51	78.16	97.90	84.92	101.46

Calcite (Table 3) shows no chemical changes at 700°C. The maximum MgO content is 1.04 wt %. Trace amounts of Fe, Si, Al, and Mn are also detected in calcite (as well as in dolomite). At 800°C both carbonates are fully transformed either into burnt lime (CaO) or into a mixture of burt lime and periclase (MgO) (*e.g.*, analysis C14). Gehlenite-like compositions are detected in some analyses (*e.g.*, C10). At 1100°C, the presence of newly formed phases, in particular wollastonite, is clearly confirmed (*e.g.*, C17). Ca content in the lime plus periclase mixture is reduced significantly due to the incorporation of this element into newly formed high-*T* silicate phases. As *T* increases, a clear compositional trend toward Si- and Al-rich calcium phases (*i.e.*, toward gehlenite and anorthite) is observed (Fig. 6a), a fact consistent with XRD and SEM-EDX results. A clear trend toward wollastonite-like compositions as well as a trend toward MgO rich composition is also observed as *T* increases (Fig. 6b). Some EMPA analyses suggest a larnite-like composition. However, XRD results do not show the presence of larnite.

3.6. XRF analysis

According to the classification proposed for clay materials in ceramic industry by Fabbri & Fiori (1985), G raw material composition falls into the quartz-feldspar sands category, while V samples fall out of any defined category due to their low silica and high calcium contents (Table 4). As expected, firing does not affect major element concentration in the brick. The only significant change is detected in the loss on ignition values. It is evidenced that G samples lost almost all water between 700 and 900°C, while V samples show a

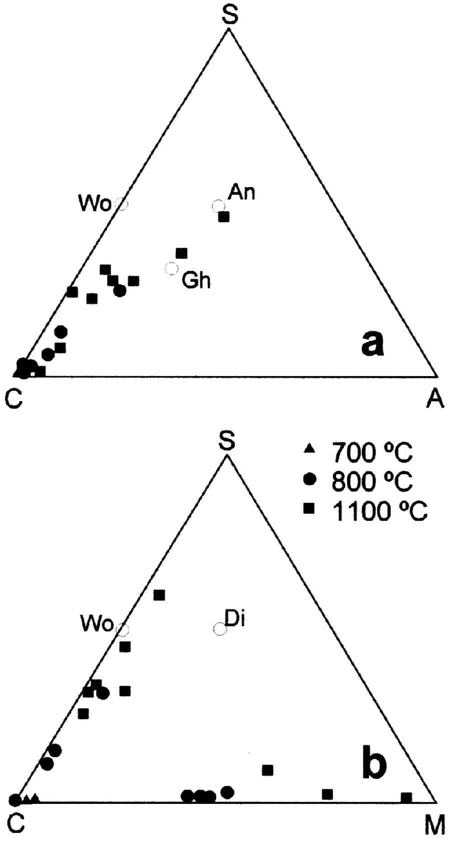

Fig. 6. a) ACS (Al_2O_3-CaO-SiO_2) and b) CMS (CaO-MgO-SiO_2) compositional diagrams of carbonates and reaction products (EMPA results).

more gradual loss of water and CO_2 as T increases (Table 4).

4. Discussion

Firing up to 700°C induce no significant mineralogical/textural transformations in both, the carbonate-rich V and the silicate-rich G samples, with the exception of the clay minerals. Clay minerals structure is reported to collapse due to dehydroxylation to resemble an illite-like structure (XRD data) when a T between 450 and 550°C is reached (Evans & White, 1958). A dehydroxylated phyllosilicate phase, structurally different to the hydrated one (Guggenheim *et al.*, 1987), is reported to exist up to 950°C when complete breakdown of the dehydroxylated illite occurs (Peters & Iberg, 1978). Our data indicate that dehydroxylation is not completed at T ~ 900°C, which indicates that the kinetics of this process is slower than previously estimated (Evans & White, 1958). $(OH)^-$ released at T > 700°C may play a significant role in texture and mineral evolution at high-T, as will be discussed later. On the other hand, muscovite shows a slight K deficit at 700°C, probably due to the high diffusion capacity of this element along muscovite (001) basal planes at T > 500°C (Sanchez-Navas & Galindo-Zaldivar, 1993). Sanchez-Navas (1999) showed high-T K-diffusion-out of mica is induced by water adsorbed along mica basal planes resulting from phyllosilicate dehydroxylation.

XRD data shows that dolomite most intense Bragg peak in V bricks, significantly reduced its intensity due to thermal decomposition at lower T than calcite main Bragg peak (Fig. 3b). Dolomite

Table 4. Bulk composition of Guadix (G) and Viznar (V) samples (XRF results in wt %).

sample	SiO_2	Al_2O_3	Fe_2O_3	MnO	MgO	CaO	Na_2O	K_2O	TiO_2	P_2O_5	LOI
G (raw)	61.95	19.76	7.37	0.10	0.77	0.57	0.90	2.85	1.05	0.17	5.15
G7 (700°C)	65.20	20.25	7.63	0.09	0.79	0.57	0.82	2.95	1.07	0.16	1.24
G8 (800 °C)	64.97	20.83	7.68	0.10	0.70	0.47	0.91	3.00	1.07	0.19	0.81
G9 (900 °C)	65.80	20.27	7.61	0.09	0.82	0.74	0.92	2.95	1.10	0.16	0.33
G10 (1000°C)	65.36	19.87	7.65	0.10	0.85	0.73	1.57	2.97	1.07	0.17	0.42
G11 (1100°C)	66.14	20.13	7.51	0.10	0.81	0.69	0.85	2.95	1.07	0.16	0.23
V (raw)	48.73	14.90	5.64	0.08	3.30	9.92	0.74	2.63	0.79	0.14	12.99
V7 (700°C)	51.70	15.27	5.82	0.08	3.54	10.69	0.78	2.67	0.77	0.14	8.24
V8 (800 °C)	55.05	16.20	6.09	0.09	3.68	11.48	0.68	2.86	0.79	0.15	3.10
V9 (900 °C)	55.83	16.20	6.08	0.08	3.69	11.45	0.84	2.86	0.85	0.15	1.18
V10 (1000°C)	56.44	16.14	6.09	0.08	3.73	11.30	0.66	2.89	0.82	0.14	1.25
V11 (1100°C)	56.18	16.20	6.16	0.08	3.71	11.63	0.98	2.91	0.86	0.14	0.28

LOI: loss on ignition.

starts to decompose according to (1) at ~ 700°C (1 atm pressure), while calcite decomposes at higher T (830 – 870°C) according to (3) (Boynton, 1980). Shoval (1988) proposed a two steps thermal decomposition for dolomite involving formation of periclase and calcite (2), followed by calcite decomposition at higher T (3).

$$\overset{\text{dolomite}}{CaMg(CO_3)_2} \rightarrow \overset{\text{lime}}{CaO} + \overset{\text{periclase}}{MgO} + 2CO_2 \qquad (1),$$

$$CaMg(CO_3)_2 \rightarrow \overset{\text{calcite}}{CaCO_3} + MgO + CO_2 \qquad (2),$$

$$CaCO_3 \rightarrow CaO + CO_2 \qquad (3).$$

However, our XRD results showing no increase in calcite 104 Bragg peak intensity as dolomite decomposes at 700°C (Fig. 3b), are not consistent with Shoval´s two-steps process.

Carbonate decomposition results in shrinkage of the brick (Barahona *et al.*, 1985). Upon storage at 22°C and 55 % RH, burnt lime (CaO) readily transforms into portlandite according to the following reaction (Boynton, 1980):

$$CaO + H_2O \rightarrow \overset{\text{portlandite}}{Ca(OH)_2} \qquad (4).$$

This process generates crystallization pressure in confined spaces (*i.e.*, the brick pores originally occupied by CaO), resulting in crack development (as observed in Fig. 2a). The dark-color rim around former carbonate grains (Fig. 5c) is probably due to limited portlandite carbonation in the presence of CO_2 also resulting in volume increase (Moorehead, 1985) and crack development (Butterworth & Honeyborne, 1952). As a common practice to avoid these undesired side-effects, bricks that contain carbonates were traditionally immersed in water to dissolve and eliminate existing CaO or $Ca(OH)_2$.

This effect is less evident in the case of MgO. Periclase in the presence of H_2O (room T) undergoes a slow transformation (it takes months or even years: Webb, 1952) into brucite ($Mg(OH)_2$), and may eventually transform into hydromagnesite ($Mg_5(CO_3)_4(OH)_2.4H_2O$), according to the following reactions (Garavelli *et al.*, 1990);

$$MgO + H_2O \rightarrow Mg(OH)_2 \qquad (5),$$

$$5Mg(OH)_2 + 4CO_2 \rightarrow \overset{\text{hydromagnesite}}{Mg_5(CO_3)_4(OH)_2.4H_2O} \qquad (6).$$

EMPA results indicate the presence of Ca and Mg oxides, however, our XRD results do not clearly show the presence of Ca and Mg oxides or hydroxides, mainly due to their low concentrations (< 10 wt %) and because their main diffraction peaks are masked by other major phase peaks (*e.g.*, quartz, feldspars, hematites). The hydromagnesite main Bragg peak at 5.81 Å is not present either.

At $T \geq 800$°C and in the absence of carbonates, changes are constrained to textural modifications and reactions where a low-T phase is decomposed and fully transformed into a high-T phase without major compositional changes (Riccardi *et al.*, 1999). In particular, muscovite undergoes a solid-state phase change into a mixture of mullite and K-feldspar (or a melt) at T ranging from 800 to 1000°C. The composition of high-T muscovite is close to K-feldspar (EMPA results), although OM analysis points to the presence of mullite. Brearley (1986) and Worden *et al.* (1987) showed fine intergrowth of alternating nanometer up to a few micrometers thick bands of K-feldspar (or a melt with composition close to that of K-feldspar) and mullite in pyrometamorphic muscovite which can explain our EMPA results.

The most significant textural and mineralogical changes are observed in samples with carbonates when fired at T > 800°C. Also, melting T and extent seems to be connected with the presence or absence of carbonates. In general, melting starts at lower T (~ 800°C) when carbonates are present (Tite & Maniatis, 1975). Ca and Mg from carbonates may act as melting agents (Segnit & Anderson, 1972), but they are reported to somehow limit the extent of vitrification at $T > 1000$°C (Everhart, 1957; Núñez *et al.*, 1992). In fact, we observed that vitrification is more extended at higher T when no carbonates exist. This may be explained considering that the phyllosilicate in the matrix of non-carbonate G samples, not contributing to the formation of high-T Ca (or Mg) silicates, and releasing significant amounts of H_2O due to dehydroxylation, they can contribute to extensive melting at high-T as demonstrated by Brearley & Rubie (1990). On the other hand, the higher SiO_2 content in these samples provides a higher amount of potential silicate-rich melt.

BSE images of reaction rims between carbonates and silicates show that formation of Ca-silicates starts at 800°C. This is confirmed by XRD (Fig. 3b) and EMPA analyses (Table 3). Gehlenite starts to form at this T by grain-boundary reaction between CaO, Al_2O_3 and SiO_2, the first deriving from former carbonates and the later two from already dehydroxylated phyllosilicates (*i.e.*, a somehow amorphous mixture of $3SiO_2.Al_2O_3$ according to Peters & Iberg, 1978), as follows,

$$\overset{\text{illite}}{\mathrm{KAl_2(Si_3Al)O_{10}(OH)_2}} + \overset{\text{calcite}}{\mathrm{6CaCO_3}} \rightarrow \overset{\text{gehlenite}}{\mathrm{3Ca_2Al_2SiO_7}} + \mathrm{6CO_2} + \mathrm{2H_2O} + \mathrm{K_2O} + \mathrm{3SiO_2} \qquad (7).$$

The formation of gehlenite is striking because one could expect the formation of an Al-rich pyroxene such as fassaite (Dondi *et al.*, 1998). Nevertheless, it should be indicated that gehlenite formation is a good example of the so-called Goldsmith´s "ease of crystallization" principle, which states that a silicate phase with all Al in 4-coordination is easier to form (at least in the lab) than a phase that includes Al in both 4- and 6-coordination when $(OH)^-$ are not present (Goldsmith, 1953). This is due to the higher energy barrier necessary to overcome when Al has to enter in a 6-coordination if compared with a 4-coordination. If $(OH)^-$ are present this energy barrier is reduced due to the smaller electrostatic repulsion among $(OH)^-$ groups than among O^{2-} in octahedral coordination. Gehlenite has all Al in tetrahedral coordination (Warren, 1930), therefore crystallizing preferentially if compared with other anhydrous Ca-Al silicates. This simple principle also applies to the high-*T* formation of other anhydrous Al-silicates as we will discuss later.

Wollastonite formed at the carbonate-quartz interface through the following reaction,

$$\mathrm{CaO} + \mathrm{SiO_2} \rightarrow \overset{\text{wollastonite}}{\mathrm{CaSiO_3}} \qquad (8).$$

Wollastonite and gehlenite appear at 800°C, a *T* ~100°C lower than previously reported (Peters & Iberg, 1978; Dondi *et al.*, 1998). This is probably due to: a) the low resolution of the analytical techniques used in the past (*i.e.*, XRD) which did not allow the detection of the small initial reaction rim between carbonates and silicates, as it is evidenced by BSE images and EMPA analyses; and/or, b) most previous works on high-*T* phase formation in ceramic processing use single components as reactants without considering additional phases or previous reaction by-products (Peters & Iberg, 1978). We observed that in a closer-to-reality multicomponent system, where interactions between reactants and products occur, different formation *T* are obtained.

At the dolomite-quartz interface, diopside starts to form at 900°C by the following reaction,

$$\mathrm{2SiO_2} + \overset{\text{dolomite}}{\mathrm{CaMg(CO_3)_2}} \rightarrow \overset{\text{diopside}}{\mathrm{CaMgSi_2O_6}} + \mathrm{2CO} \qquad (9).$$

At this *T*, anorthite starts to form at the expenses of calcite and illite (plus quartz),

$$\overset{\text{illite}}{\mathrm{KAl_2(Si_3Al)O_{10}(OH)_2}} + \overset{\text{calcite}}{\mathrm{2CaCO_3}} + \mathrm{4SiO_2} \rightarrow \overset{\text{K-feldspar}}{\mathrm{2KAlSi_3O_8}} + \overset{\text{anorthite}}{\mathrm{2Ca_2Al_2SiO_8}} + \mathrm{2CO_2} + \mathrm{H_2O} \qquad (10).$$

At higher temperatures (1000 to 1100°C), phyllosilicates have already disappeared in all samples (V and G), being transformed into sanidine and mullite plus a melt according to the following reaction,

$$\overset{\text{illite (muscovite)}}{\mathrm{3KAl_2(Si_3Al)O_{10}(OH)_2}} + \mathrm{2SiO_2} \rightarrow \overset{\text{sanidine}}{\mathrm{3KAlSi_3O_8}} + \overset{\text{mullite}}{\mathrm{Al_6Si_2O_{13}}} + \mathrm{3H_2O} + \text{melt} \qquad (11).$$

Formation of a melt during the previous reaction (Brearley & Rubie, 1990) is consistent with the observed "cellular structure" of muscovite (Tite & Maniatis, 1975).

Brearley (1986) proposed a somehow different reaction for mullite formation at the expenses of phengitic muscovite, resulting in K-feldspar + mullite + biotite. No biotite is detected in our experiments, most probably due to the low Fe content in V and G micas. Brearley & Rubie (1990) experimentally demonstrated that high-*T* muscovite breakdown in the presence of quartz is influenced by the crystal size. The smallest crystals have a strong tendency to react with H_2O, resulting in enhanced melt formation, while large muscovite crystals form limited amounts of melt. This may account for the significant vitrification of the matrix (specially in G samples), while large muscovite grains (up to some mm in size) still do not show significant melting.

Mullite, which according to OM analysis first appears at 800°C, is the second most abundant phase (after quartz) at 1100°C in the richer in phyllosilicate G samples. It is interesting to mention that K-feldspar progressively disappears as *T* increases. This is not consistent with published data (Maggetti, 1982). It seems that low-*T* K-feldspar (microcline) is not stable at high-*T*, therefore, it transforms into a high-*T* K-feldspar (*i.e.*, sanidine) or reacts with lime to form anorthite. Both, sanidine and anorthite, are detected in the high-*T* bricks. However, a higher concentration of sanidine should be expected to form, specially considering reaction (11). A possible explanation for the low K-feldspar content at high-*T* is that K-feldspar might not have enough time to develop its crystalline structure (sanidine), therefore being concentrated as an amorphous (sanidine-like) phase responsible in part for the rise in the background noise in the XRD results. Mullite formation seems to be kinetically faster, resulting in a well-developed crystalline phase, which gives sharp diffraction peaks. Goldsmith (1953) indicates that mullite could be another example of his "simplexity principle" for the "ease" of crystallization, if compared with other aluminum silicates. In fact, the mullite structure has a larger amount of Al in 4-coordination and less Al in 6-coordination than sillimanite (Rehak *et al.*, 1998) for instance, which may account for the abundance of the former and the non-existence of the latter in the studied bricks.

In carbonate-rich V samples fired at $T >$ 1000°C a significant reduction of gehlenite main diffraction peak is observed. According to Peters & Iberg (1978) this is due to the reaction of this phase with quartz, forming wollastonite and anorthite. This is consistent with the increase in the main Bragg peak intensity of these later minerals at 1100°C.

At the dolomite-silicate (*i.e.*, Qtz and Phy) interface it is common to observe wollastonite, either newly formed or resulting from the destruction of gehlenite. The texture of the interface is rather complex. Protrusion or fingers from the reaction zone penetrate into areas were complete transformation into wollastonite has occurred. The interface geometry resembles the so-called "viscous fingers" (Garcia-Ruiz, 1992), occurring when two fluids or semi-plastic solids of different composition and viscosity are placed in contact. Initially, the contact zone is a flat surface, but later on, it reaches a fingered fractal geometry (Nittmamm *et al.*, 1985). In the carbonate-silicate interface a similar process may have taken place, where mass transport of the reactants may have been enhanced by partial melting. The formation of a silicate-rich melt due to clay-minerals melting (Brearley & Rubie, 1990) in the external part of the ring in contact with a second inner melt formed by preexisting gehlenite or the eutectic $CaO\text{-}SiO_2$, would result in viscous finger development. The fractal geometry of the developing viscous fingers may have enhanced diffusion of mobile ions such as Ca toward silicate reactive sites. Both, EDX data showing Mg enrichment in the dolomite core (Fig. 5f), and the compositional trend towards MgO-rich terms in the CMS diagram (Fig. 6b) confirm that Ca is preferentially leached out of the former dolomite grain. Finger formation will result in a significant increase in interface surface area, resulting in higher reaction rates. Another alternative explanation for this fingered geometry development involves partial melting at the carbonate-silicate interface, and mass transport (*i.e.*, viscous flow) through the clay-quartz porous matrix, resulting in the so-called "scalloped structure" proposed by Ortoleva *et al.* (1987) for reaction-diffusion processes. While the viscous finger model requires two melts, the second model only requires one melt. It is not clear if at any moment conditions for two melt occurrence are reached. Hence, the second model seems more plausible.

In any case, the process which is originally diffusion driven, is transformed into a mass (*i.e.*, fingering) plus diffusion transport which greatly enhances Ca-silicate formation. This is consistent with the thick reaction rims (up to 250 µm thick; see Fig. 5f) that surround former carbonate grains. These thick Ca-silicate shells would hardly develop just by diffusion in the short time-scale of the experiment (3 hours at the peak T). In fact, at 800°C (conditions where melting would be very limited) Ca (and Mg)-silicate rims formed around calcite or dolomite are 2-5 µm thick. At 1100°C when melting is extensive, the reaction rate is so high that rims are two orders of magnitude thicker. Therefore, mass transport (*i.e.*, viscous flow) seems to have played a key role in high-T Ca-(Mg-) silicate formation. Mass transport is also consistent with observation of some areas with different composition (unreacted silicates) trapped between fingers, resulting in the island geometry observed in Fig. 5g. It could be expected that without fingering, the process of Ca- or (Ca-Mg)-silicate formation would be self-limiting: *i.e.*, once a rim of the newly formed silicate appears, diffusion would be jeopardized. This shell would preclude or limit the transport of Ca (and/or Mg) from the carbonate, or it would limit the transport of the less mobile Si (and Al) from the surrounding silicate towards the reaction front. Therefore, it is necessary that one of the above described transport-reaction mechanisms takes place. This may also explain why phase formation takes place at lower T than reported previously. The presence of multiple interfaces among different crystals may enhance finger development, resulting in kinetic changes favoring phase formation at lower T.

5. Conclusions

It is observed that even though the overall composition of a ceramic material does not undergo major changes upon firing, significant mineralogical and textural modifications do occur.

These changes are connected with two reaction types: a) solid-state replacement of a phase by a new one with little or no compositional variation (*i.e.*, the muscovite and illite case) and minimizing energy changes by preserving the original texture and orientation of the replaced phase; and b) reaction-diffusion at the interface between two mineral grains with contrasting composition (*i.e.*, carbonate-silicate interfaces). The latter reaction is enhanced if mass/viscous transport resulting from partial melting and finger structure development occurs. Non-carbonated clay-rich materials (G) show phyllosilicate destruction at *T* ranging from 700 to 900°C, followed by vitrification which is significant at $T > 1000$°C. Carbonate-rich materials (V) show major phase transformation upon phyllosillicates destruction, including new Ca (or Mg) silicates and aluminum-silicates formation. In this later case, the vitrification starts at lower *T* and it is limited at higher *T*. Therefore, it is possible to establish the firing *T* of ceramic materials with composition broadly similar to that in our work, based on the mineralogy. Thus: a) presence of phyllosilicates indicates a low 700 to 900°C firing *T* for the dehydroxylated illite (or muscovite) phase; b) dolomite disappears at ≥ 700°C, while calcite is still present at 800°C; c) gehlenite appears at 800°C, reducing its concentration above 1000°C; d) diopside and wollastonite appear at 800°C (in very low concentrations) as reaction rims between carbonates and silicates. Formation of these minerals includes "fingering" development; e) mullite appears at $T > 800$°C, while little amounts of sanidine form as microcline disappears; and f) anorthite develops at $T > 1000$°C in carbonate-rich bricks.

When considering equilibrium thermodynamic data and calculated reaction *T* for most of the above mentioned phases and reactions (Holland & Powell, 1985, and references herein), it is observed that rapid heating induces significant overstepping. Therefore, phases formed are in most cases metastable, a fact consistent with analyses of pyrometamorphic assemblages (Brearley & Rubie, 1990, and references herein).

The formation of non-equilibrium fractal morphologies at the carbonate-silicate reaction interfaces may explain why high-*T* silicates in carbonate-rich ceramics develop very fast. This grain-to-grain reaction model may help explain high-*T* silicate formation in nature (*e.g.*, contact metamorphism, pyrometamorphism in xenoliths).

The gained knowledge on mineral transformation and the dynamics of interface mass and diffusion transport facilitated through "fingering" or "scalloping" opens new ways to understand the complexities of ceramic processing in particular and high-*T* mineral transformation in general, both in natural (*i.e.*, geologic settings) and artificial contexts (*e.g.*, archaeometric analysis of ancient ceramics, or the design of new bricks –replicas of ancient ones– for architectural heritage conservation). However, care must be taken when extrapolating these results to other raw material compositions and/or ceramic processing methods.

Acknowledgements: This work has been financially supported by the CGICYT project MAT2000-1457 and the Research Group RNM 0179 of the Junta de Andalucía (Spain). We thank the Centro de Instrumentación Cientifica (CIC) of the Granada University for allowing us to use their SEM-EDX, EMPA, and XRF facilities. We thank K. Elert, J.M. García-Ruiz, M. Rodriguez-Gallego, and A. Sanchez-Navas for fruitful discussions and comments. We also thank the in-depth review by Dr. F. Götz-Neunhoeffer and an anonymous referee.

References

Barahona, E., Huertas, F., Pozzuoli, A., Linares, J. (1985): Firing properties of ceramic clays from Granada province, Spain. *Miner. Petrogr. Acta*, **29A**, 577-590.

Boynton, R.S. (1980): Chemistry and technology of lime and limestone, 2nd Ed., Wiley, New York.

Brearley, A.J. (1986): An electron optical study of muscovite breakdown in pelitic xenoliths during pyrometamorphism. *Miner. Mag.*, **357**, 385-397.

Brearley, A.J. & Rubie, D.C. (1990): Effects of H_2O on the disequilibrium breakdown of muscovite + quartz. *J. Petrol.*, **31**, 925-956.

Butterworth, B. & Honeyborne, D.B. (1952): Bricks and clays of the hasting beds. *Trans. Brit. Ceram. Soc.*, **51**, 211-259.

Dondi, M., Ercolani, G., Fabbri, B., Marsigli, M. (1998): An approach to the chemistry of pyroxenes formed during the firing of Ca-rich silicate ceramics. *Clay Minerals*, **33**, 443-452.

Duminuco, P., Riccardi, M.P., Messiga, B., Setti, M. (1996): Modificazioni tessiturali e mineralogiche come indicatori della dinamica del processo di cottura di manufatti ceramici. *Ceramurgia*, **26**, 5, 281-288.

Evans, J.L. & White, J. (1958): Further studies of the thermal decomposition of clays. *Trans. Brit. Ceram. Soc.*, **57**, 6, 298.

Everhart, J.O. (1957): Use of auxiliary fluxes to improve structural clay bodies. *Bull. Am. Ceram. Soc.*, **36**, 268-271.

Fabbri, B. & Fiori, C. (1985): Clays and complementary raw materials for stoneware tiles. *Miner. Petrogr. Acta*, **29-A**, 535-545.

Freestone, I.C. & Middleton A.P. (1987): Mineralogical applications of the analytical SEM in archaeology. *Miner. Mag.*, **51**, 21-31.

Garavelli, C.L., Liviano, R., Vurro, F., Zinco, M. (1990): Idromagnesite nei materiali di rivestimento della chiesa ipogea di S. Maria della Grazia (Laterza, Puglia), *in* "Superfici dell´Architetture: La Finiture". Graffo, Bressansone, 189-197.

Garcia-Ruiz, J.M. (1992): "Peacock" viscous fingers. *Nature*, **356**, 113.

Goldsmith, J.R. (1953): A "simplexity principle" and its relation to "ease" of crystallization. *Bull. Geol. Soc. Am.*, **64** , 439-451.

Govindaraju, K. (1989): 1989 compilation of working values and sample description for 272 geostandards. *Geostandards Newsletter*, Special issue, **13**, 1-113.

Guggenheim, S., Chang, Y., van Groos, A.F.K. (1987): Muscovite dehydroxylation: high-temperature studies. *Am. Mineral.*, **72**, 537-550.

Holland, T.J.B & Powell, R. (1985): An internally consistent thermodynamic dataset with uncertainties and correlations: 2. Data and results. *J. metamorphic Geol.*, **3**, 343-370.

Kretz, R. (1983): Symbols for rock-forming minerals. *Am. Mineral.*, **68**, 277-279.

Maggetti, M. (1982): Phase analysis and its significance for technology and origin, *in* "Archaeological Ceramics", Olin, J.S., ed. Smithsonian Institution Press, Boston, 121-133.

Moorehead, D.R. (1985): Cementation by the carbonation of hydrated lime. *Cement Concr. Res.*, **16**, 700-708.

Nittmamm, J., Daccord, G., Stanley, H.E. (1985): Fractal growth of viscous fingers: quantitative characterization of a fluid instability phenomenon. *Nature*, **314**, 141-144.

Núñez, R., Delgado, A., Delgado, R. (1992): The sintering of calcareous illitic ceramics. Application in archaeological research, *in* "Electron Microscopy EUREM 92", A. Galindo, ed. University of Granada, Granada, 795-796.

Ortoleva, P., Chadam, J., Merino, E., Sen, A. (1987): Geochemical self-organization II: The reactive-infiltration instability. *Am. J. Sci.*, **287**, 1008-1040.

Peters, T. & Iberg, R. (1978): Mineralogical changes during firing of calcium-rich brick clays. *Ceram. Bull.*, **57**, 5, 503-509.

Preston, B.J., Dempster, T.J., Bell, B.R., Rogers, G. (1999): The petrology of mullite-bearing peraluminous xenoliths: Implications for contamination processes in basaltic magmas. *J. Petrol.*, **40**, 349-473.

Rehak, P., Kunath-Fandrel, G., Losso, P., Hildmann, B., Schneider, H., Jäger, C. (1998): Study of the Al coordination in mullites with varying Al:Si ratio by 27Al NMR spectroscopy and X-ray diffraction. *Am. Mineral.*, **83**, 1266-1276.

Riccardi, M.P., Messiga, B., Duminuco, P. (1999): An approach to the dynamics of clay firing. *Appl. Clay Sci.*, **15**, 393-409.

Rye, O.S. (1976): Keeping your temper under control: Materials and Manufacture of Papuan Pottery. *Archeology and Phys. Anthropology in Oceania*, **11**, 12, 106-137.

Sanchez-Navas, A. (1999): Sequential kinetics of a muscovite-out reaction: A natural example. *Am. Mineral.*, **84**, 1270-1286.

Sanchez-Navas, A. & Galindo-Zaldivar, J. (1993): Alteration and deformation microstructures in biotite from plagioclase-rich dykes (Ronda Massif, S. Spain). *Eur. J. Mineral.*, **5**, 245-256.

Scott, V.D. & Love, G. (1983): Quantitative Electron-Prove Microanalysis. John Wiley & Sons, New York.

Segnit, E.R. & Anderson, C.A. (1972): Scanning electron microscopy of fired illite. *Trans. Brit. Ceram. Soc.*, **71**, 85-88.

Shoval, S. (1988): Mineralogical changes upon heating calcitic and dolomitic marl rocks. *Thermochim. Acta*, **135**, 243-252.

Tite, M.S. & Maniatis, Y. (1975): Examination of ancient pottery using the scanning electron microscope. *Nature*, **257**, 122-123.

Veniale, F. (1990): Modern techniques of analysis applied to ancient ceramics, *in* "Advanced Workshop on Analytical Methodologies for the Investigation of Damaged Stones", F. Veniale and U. Zezza, eds., University of Pavia, Pavia, 1-45.

Warren, B.E. (1930): The structure of melilite $(Ca,Na)_2(Mg,Al)_1(Si,Al)_2O_7$. *Zeits. Kristall.*, **74**, 131-138.

Webb, T.L. (1952): Chemical aspects of the unsoundness and plasticity in building limes. *The South African Industrial Chemist*, 290-294

Worden, R.H., Champness, P.E., Droop, G.T.R. (1987): Transmission electron microscopy of pyrometamorphic breakdown of phengite and chlorite. *Mineral. Mag.*, **51**, 107-121.

Received 20 February 2000
Modified version received 12 July 2000
Accepted 8 January 2001